Technical Report 493

J. W. Modestino

A Model for ELF Noise

16 December 1971

Prepared for the Department of the Navy
under Electronic Systems Division Contract F19628-70-C-0230 by

Lincoln Laboratory

MASSACHUSETTS INSTITUTE OF TECHNOLOGY

Lexington, Massachusetts

DOCUMENT CONTROL DATA – R&D

(Security classification of title, body of abstract and indexing annotation must be entered when the overall report is classified)

1. ORIGINATING ACTIVITY *(Corporate author)* Lincoln Laboratory, M.I.T.	2a. REPORT SECURITY CLASSIFICATION Unclassified 2b. GROUP None

3. REPORT TITLE

A Model for ELF Noise

4. DESCRIPTIVE NOTES *(Type of report and inclusive dates)*

Technical Report

5. AUTHOR(S) *(Last name, first name, initial)*

Modestino, James W.

6. REPORT DATE 16 December 1971	7a. TOTAL NO. OF PAGES 30	7b. NO. OF REFS 10
8a. CONTRACT OR GRANT NO. F19628-70-C-0230 b. PROJECT NO. 1508A c. d.	9a. ORIGINATOR'S REPORT NUMBER(S) Technical Report 493 9b. OTHER REPORT NO(S) *(Any other numbers that may be assigned this report)* ESD-TR-71-322	

10. AVAILABILITY/LIMITATION NOTICES

Approved for public release; distribution unlimited.

11. SUPPLEMENTARY NOTES None	12. SPONSORING MILITARY ACTIVITY Department of the Navy

13. ABSTRACT

A model for ELF atmospheric noise is proposed and studied in detail. The model is completely described by a few meaningful parameters which are easily correlated with measured data. Procedures for fitting the free parameters to observed noise data are provided. The model should prove useful in the analysis and design of communication systems operating in impulsive noise environments.

14. KEY WORDS

ELF noise
atmospheric noise
impulsive noise
non-Gaussian noise

MASSACHUSETTS INSTITUTE OF TECHNOLOGY

LINCOLN LABORATORY

A MODEL FOR ELF NOISE

J. W. MODESTINO

Consultant to Group 66

TECHNICAL REPORT 493

16 DECEMBER 1971

LEXINGTON MASSACHUSETTS

The work reported in this document was performed at Lincoln Laboratory, a center for research operated by Massachusetts Institute of Technology. The work was sponsored by the Department of the Navy under Air Force Contract F19628-70-C-0230.

ABSTRACT

A model for ELF atmospheric noise is proposed and studied in detail. The model is completely described by a few meaningful parameters which are easily correlated with measured data. Procedures for fitting the free parameters to observed noise data are provided. The model should prove useful in the analysis and design of communication systems operating in impulsive noise environments.

Accepted for the Air Force
Joseph R. Waterman, Lt. Col., USAF
Chief, Lincoln Laboratory Project Office

CONTENTS

	Abstract	iii
I.	Introduction	1
II.	Characteristics of ELF Noise	1
III.	Proposed Model	7
IV.	Digital Realization of Model for ELF H-Field Noise	13
V.	Choice of Parameter Values	15
VI.	Summary and Conclusions	23
References		23

A MODEL FOR ELF NOISE

I. INTRODUCTION

The primary source of electromagnetic noise at ELF (3 to 300 Hz) can be attributed to lightning discharges which propagate in the earth-ionosphere cavity. As a result, the received noise at a typical ELF receiving site tends to be impulsive in character even in the absence of strong local thunderstorm activity. Furthermore, ELF noise has been observed to exhibit strong geographical, seasonal, and diurnal dependence so that the observed noise background can be expected to be non-stationary as well as highly non-Gaussian. To assess the performance of communication systems operating in such environments, it is important to have available a mathematical model that provides a complete statistical description of the received noise. It might be added that this requirement exists whether the problem is that of obtaining results on system performance analytically or by computer simulation. To be useful, any such model must satisfy the following diserata:

(a) It must agree reasonably well with the underlying physics.

(b) It must be completely describable by a few meaningful parameters.

(c) Its statistical characterization must be easily correlated with corresponding measured data.

(d) Hopefully it is mathematically tractable.

The present report is one of a series concerned with the development and application of such a model to ELF communications. In this report we will be concerned with the development of this model and the fitting of its parameters to observed ELF noise. Other reports in this series will be concerned with optimum/suboptimum receiver structures and their digital realizations.

Before entering upon a detailed discussion of this model, let us briefly review some of the pertinent characteristics of ELF noise.

II. CHARACTERISTICS OF ELF NOISE

General observations of wideband ELF noise reveal frequent occurrences of large pulses superimposed upon a more homogeneous appearing background noise. Typical recorded* H-field noise waveforms are illustrated in Figs. 1 through 3. We have found it convenient to classify the recorded noise into the three categories: high, moderate, and low-level, depending upon the observed spectral levels. An exception is the case of Norway data which appear to be of a uniform level. The large pulses present in the waveforms of Figs. 1 through 3 are undoubtedly due to strong local thunderstorm activity while the background structure, on the other hand, is due to a considerably greater number of unresolved low-level pulses attributed to more remote thunderstorm activity. As a result, it follows from central limit theorem considerations that the large number of low-level overlapping pulses resemble Gaussian noise. Considerable departures from this condition are to be expected at larger amplitudes. Indeed, measurements of the amplitude probability distribution (APD) of ELF noise confirm this. Figures 4 through 6 illustrate the computed APD's corresponding to the noise waveforms appearing in Figs. 1 through 3. Here we are plotting the probability or percent of time that the absolute value of the recorded noise exceeds a given level measured in rms units. The scales have been chosen so that the APD of Gaussian noise plots as a straight line of slope $-\frac{1}{2}$ as illustrated in Fig. 7. From

*The details of the measurement and recording system are described in Ref. 1.

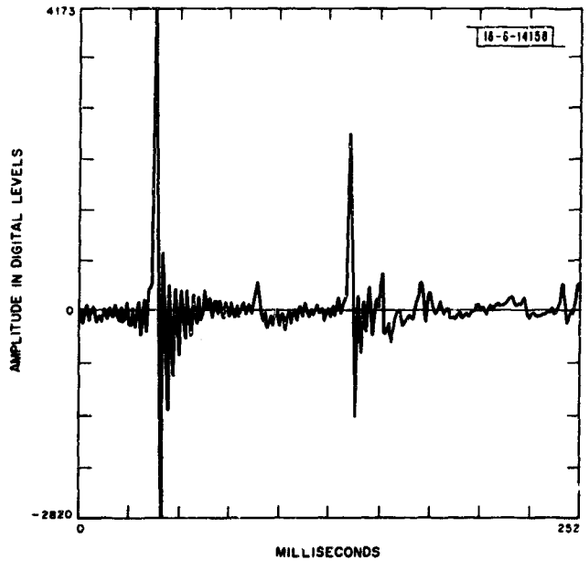

Fig. 1. Typical high-level H-field ELF noise waveform recorded at Saipan.

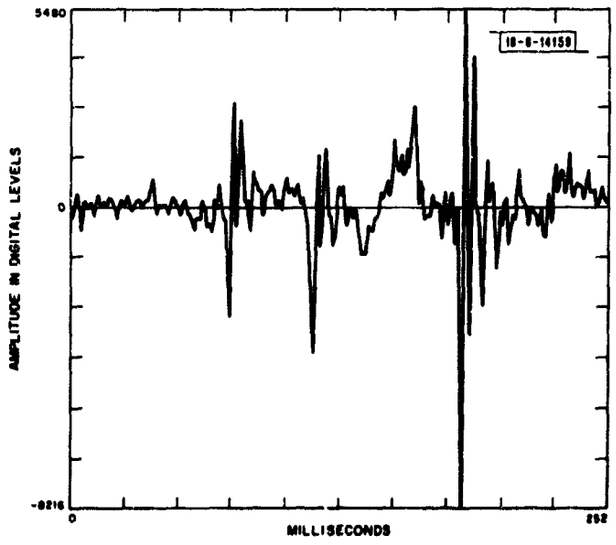

Fig. 2. Typical moderate-level H-field ELF noise waveform recorded at Malta.

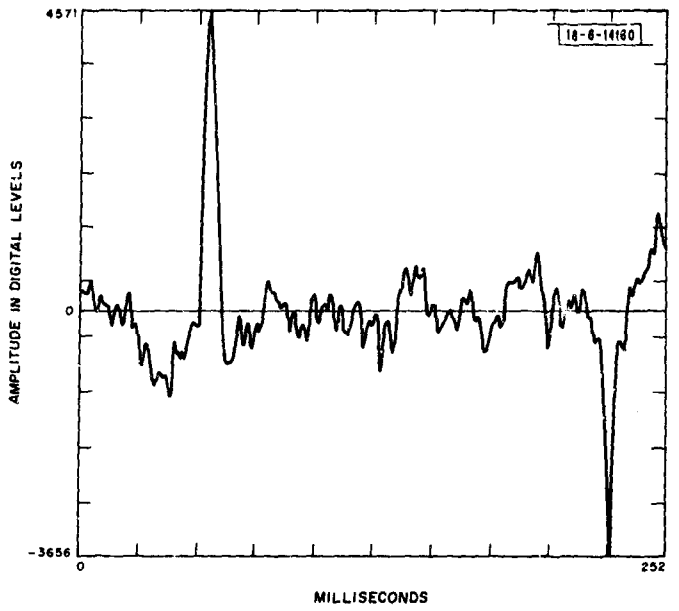

Fig. 3. Typical H-field ELF noise waveform recorded at Norway.

Figs. 4 through 6 it is to be observed that at low amplitudes the APD does indeed resemble that of Gaussian noise while exhibiting a much larger dynamic range at larger amplitude levels.

Also of interest are various first-order temporal statistics of ELF noise. We will be particularly interested in such quantities as the average number of high-level pulses per second and the distribution of the interval between their occurrences. Unfortunately, such quantities are difficult to obtain from the recorded data in any unambiguous fashion. Some techniques for the analysis and measurement of the temporal statistics of ELF noise are described in detail in Ref. 1. Here a useful criterion for the presence of a pulse in wideband ELF noise was presented in terms of three parameters T_L, T_u, and S_c, as illustrated in Fig. 8. The "beginning" of a pulse is said to have occurred when the absolute value of the noise waveform first exceeds a threshold T_u, while the "duration" of such a pulse is measured from this instant until such time as the absolute value has been below T_L for at least S_c seconds. It is clear that any practical use of measurements based upon this criterion will require careful choice of the parameters T_L, T_u, and S_c. Obviously, both T_L and T_u should be placed just above the background noise level if such a point can be accurately defined. Often this can be accomplished by observation of the APD plot. The knee of the APD plot, which represents the point of departure from Gaussian behavior, is in most cases quite pronounced (Figs. 4 through 6). Suitable thresholds taken about this point should provide useful information on the temporal statistics of the high-level pulses while excluding the low-level background noise from consideration. For definiteness we have developed the following useful procedure for placement of the threshold levels. First, draw tangents to the two distinct portions of the APD curve as illustrated by the dashed lines in Fig. 9. Let T represent the level in rms units, corresponding to the intersection of these two lines (T = −6 dB for the high-level Saipan data illustrated in Fig. 9) and set $T_u = T_L = T$. The choice of S_c, on the other hand, is not quite so straightforward. Obviously, we would like to make S_c as small as possible without causing portions of a single noise burst to be mistaken for two or more resolved pulses. From experimentation, with the noise thresholds set at the value T described above, we have found values of S_c in the range 5 to 10 msec sufficient.

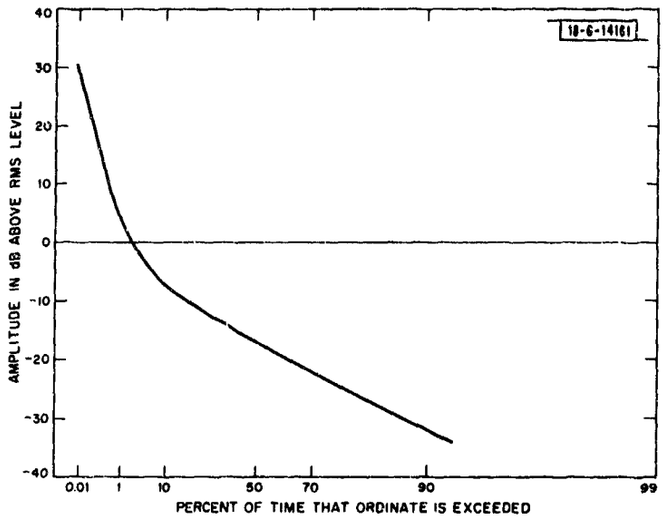

Fig. 4. APD of high-level Saipan H-field ELF noise.

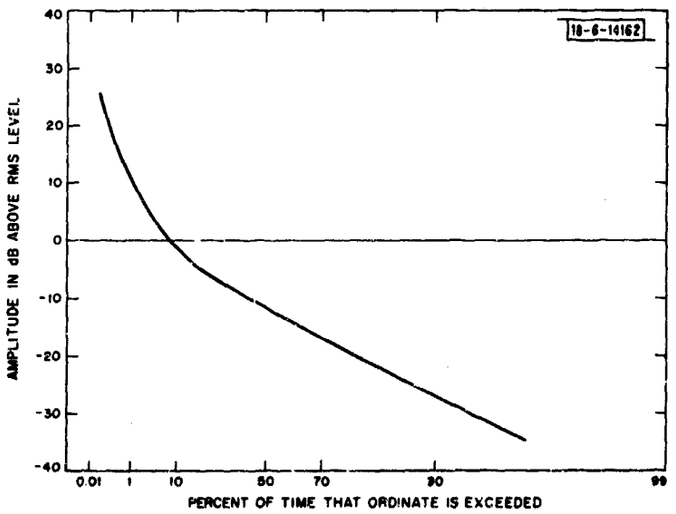

Fig. 5. APD of moderate-level Malta H-field ELF noise.

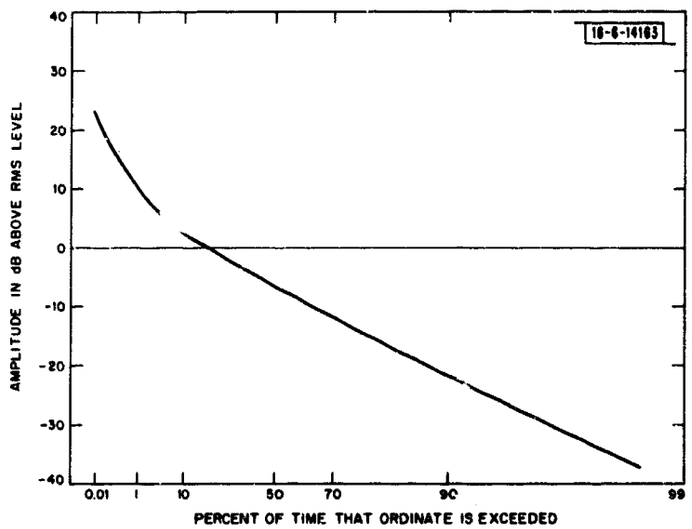

Fig. 6. APD of typical Norway H-field ELF noise.

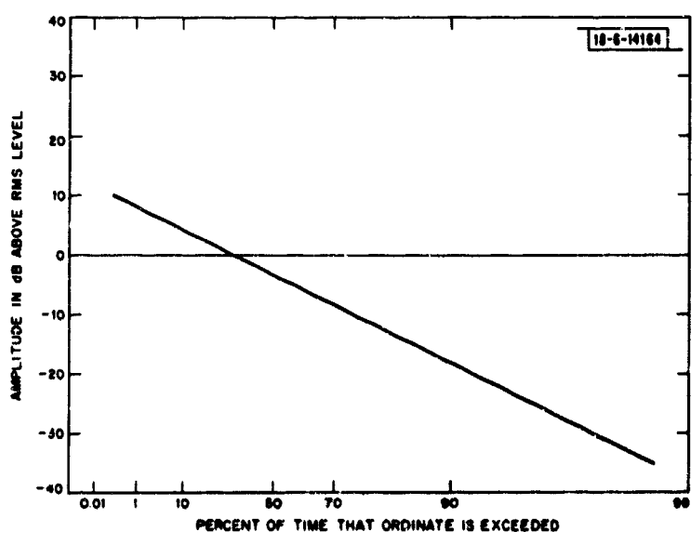

Fig. 7. APD of Gaussian noise.

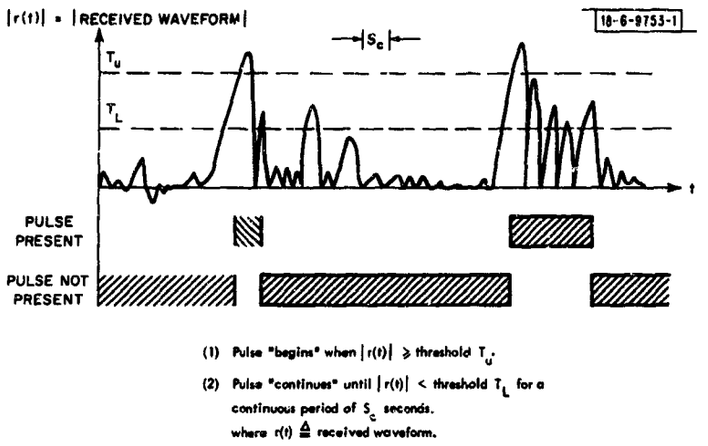

Fig. 8. Criteria defining "beginning" and "end" of wideband ELF noise pulse.

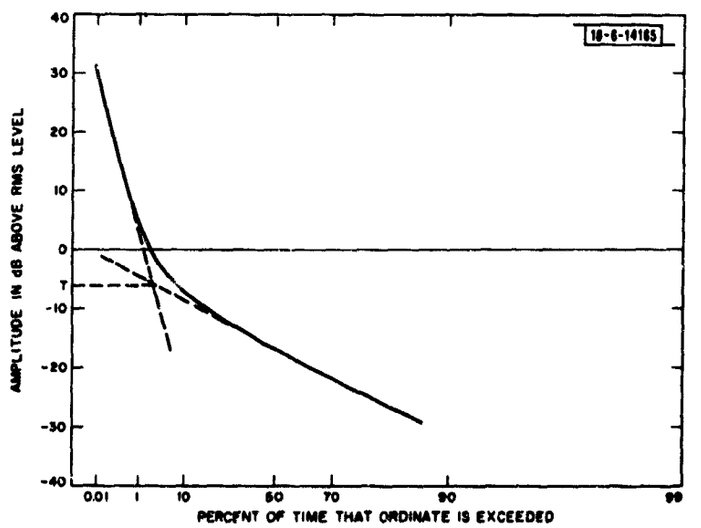

Fig. 9. Criteria for defining threshold T.

TABLE I

TYPICAL FIRST-ORDER TEMPORAL STATISTICS OF ELF NOISE

Noise Data	Average Number of Pulses/Second		Average Pulse Duration*	
	S_c = 5 msec	S_c = 10 msec	S_c = 5 msec	S_c = 10 msec
Saipan				
High-Level	12.8	10.4	4.0	7.0
Moderate-Level	10.2	8.2	5.0	8.0
Low-Level	8.0	7.6	6.0	8.0
Malta				
High-Level†				
Moderate-Level	11.3	10.8	4.0	5.0
Low-Level†				
Norway	9.3	8.5	3.0	4.0

* Duration is the actual width of the pulse obtained by subtracting the interval S_c from the definition of duration in Ref. 1.

† No data available.

Table I illustrates some typical results using the above criteria which will be of use to us later. It is of some interest that these results compare favorably with visual observations.

It should be noted at this time that it is nowhere suggested that the simple first-order amplitude and temporal statistics that we have been considering completely describe ELF noise. Nevertheless, they are useful in that any proposed model must at least result in statistics which compare favorably with these easily measured quantities.

III. PROPOSED MODEL

An intuitively satisfying model for impulsive noise processes typical of the ELF environment consists of the sum of a low-density* shot process[2,3] and Gaussian noise. The shot process accounts for the randomly occurring high-level pulses while the additive Gaussian noise represents the low-level background noise. A convenient representation for the shot process is that of a random impulse train exciting a finite-state linear (usually time invariant) system as first proposed by Synder.[4] Thus, we will assume that the noise processes of interest can be described by the state equation

$$\dot{\underline{x}}(t) = \underline{A}\,\underline{x}(t) + \underline{b}u(t) \quad ; \quad \underline{x}(t_o) = \underline{x}_o \tag{1a}$$

and the output relation

$$y(t) = \langle \underline{c}, \underline{x}(t) \rangle \quad , \tag{1b}$$

where $\underline{A}$ is a constant $n \times n$ matrix, $\underline{b}$ and $\underline{c}$ are n-vectors (specifically column vectors) and $\langle \cdot, \cdot \rangle$ denotes an inner product. The state vector $\underline{x}(t)$ is itself an n-vector while the input is a scalar of the form

$$u(t) = \sum_{i=1}^{N(t)} u_i\, \delta(t - t_i) \quad , \tag{2}$$

* By "low-density" we mean that the average inter-arrival time between exciting impulses is greater than any system time constants.

i.e., a point process. Here $\{N(t),\ t \geq 0\}$ is a counting process[5] with arrival times $t_1, t_2, \ldots$, and $\{u_i\}$ is a sequence of independent and identically distributed (i.i.d.) random variables with common univariate probability density function (p.d.f.) $f(\cdot)$. Finally, the observed noise is given by

$$n(t) = y(t) + w(t) \quad , \tag{3}$$

where w(t) is a white* zero-mean Gaussian noise process with double-sided noise spectral density $\sigma_o^2 = N_o/2$ watts/Hz and assumed independent of the driving point process u(t).

While there are many possible state-space realizations of the system described by Eq. (1) leading to the same input-output behavior,[6] the particular realization that we have adopted (mainly to agree with Ref. 7) is such that

$$\underline{\underline{A}} = \begin{bmatrix} -a_1 & 1 & 0 & . & . & . & 0 \\ -a_2 & 0 & 1 & . & . & . & 0 \\ . & . & . & . & & & . \\ . & . & . & & . & & . \\ . & . & . & & & . & . \\ -a_{n-1} & 0 & 0 & . & . & . & 1 \\ -a_n & 0 & 0 & . & . & . & 0 \end{bmatrix} \tag{4}$$

while $\underline{b}^T = (b_1, b_2, \ldots, b_n)$ and finally $\underline{c}^T = (c, 0, 0, \ldots, 0)$. The resulting system transfer function of the linear dynamical system generating the shot process is easily seen to be given by a proper rational function simply related to the coefficients of $\underline{\underline{A}}$ and $\underline{b}$, i.e.,

$$H(s) \triangleq \frac{Y(s)}{U(s)} = \langle \underline{c}, [s\underline{\underline{I}} - \underline{\underline{A}}]^{-1}\underline{b} \rangle$$

$$= \frac{b_1 s^{n-1} + b_2 s^{n-2} + \ldots b_n}{s^n + a_1 s^{n-1} + \ldots a_n} \quad , \tag{5}$$

where $\underline{\underline{I}}$ is the $n \times n$ identity matrix and U(s) and Y(s) are Laplace Transforms in the complex variable s of the input u(t) and output y(t) of the linear dynamical system. The resulting state-space realization is illustrated in Fig. 10. An alternative realization based upon the system transfer function [Eq. (5)] which will prove useful in later digital implementations can be obtained by observing[8] that the matrix $[s\underline{\underline{I}} - \underline{\underline{A}}]^{-1}$ in Eq. (5) has the spectral representation†

$$[s\underline{\underline{I}} - \underline{\underline{A}}]^{-1} = \sum_{k=1}^{n} \frac{\underline{\underline{Z}}_k}{(s - s_k)} \quad , \tag{6}$$

where the s_k, $k = 1, 2, \ldots n$ are eigenvalues of $\underline{\underline{A}}$ (poles of the system transfer function) and

* The analysis is easily extended to colored processes.

† We have assumed that the poles of the system transfer function are distinct.

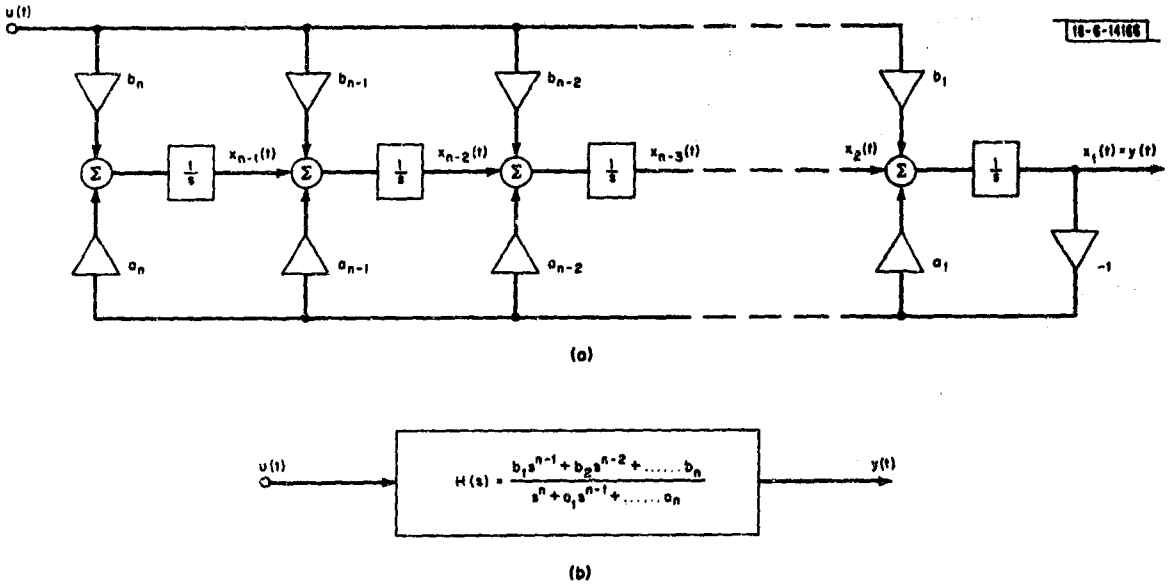

Fig. 10. Two realizations of linear dynamic system. (a) State-space realization; (b) input/output realization.

$$\underline{\underline{Z}}_k = \frac{1}{2\pi i} \oint_{C_k} [s\underline{\underline{I}} - \underline{\underline{A}}]^{-1}\, ds \quad ; \quad k = 1, 2, \ldots n \tag{7}$$

with C_k any closed contour in the complex plane enclosing only the pole at s_k. Substituting this result into Eq. (5), we obtain

$$H(s) = \sum_{k=1}^{n} \frac{A_k}{s - s_k} \quad , \tag{8}$$

where

$$A_k = \frac{1}{2\pi i} \oint_{C_k} \langle \underline{c}\,,\, [s\underline{\underline{I}} - \underline{\underline{A}}]^{-1}\underline{b} \rangle\, ds$$

$$= \frac{1}{2\pi i} \oint_{C_k} H(s)\, ds \tag{9}$$

is simply the residue of $H(s)$ at the pole s_k. Thus, Eq. (8) is merely a partial fraction expansion of the system transfer function.

We will be interested, among other things, in the amplitude probability distribution (APD) of the process $n(t)$ described by Eq. (3). To this end consider the characteristic function (ch.f.) of $n(t)$ given by

$$\psi_n(v; t) \triangleq E\{e^{ivn(t)}\}$$

$$= E\{e^{iv\langle \underline{c}\,,\, \underline{x}(t)\rangle}\}\, E\{e^{ivw(t)}\} \quad , \tag{10}$$

where we have made use of the assumed independence between the u(t) and w(t) processes. Letting

$$\psi_g(v) \triangleq E\{e^{ivw(t)}\} \tag{11}$$

and

$$\psi_y(v;t) \triangleq E\{e^{iv\langle \underline{c}, \underline{x}(t)\rangle}\} \quad , \tag{12}$$

we have

$$\psi_n(v;t) = \psi_g(v)\,\psi_y(v;t) \tag{13}$$

Note that $\psi_g(v)$ is merely the univariate ch.f. of a stationary zero-mean Gaussian process so that

$$\psi_g(v) = e^{-\frac{1}{2}\sigma_o^2 v^2} \quad , \tag{14}$$

where σ_o^2 has been described previously and is independent of t. To evaluate $\psi_y(v,t)$, note that the solution to (1a) is given by[6]

$$\underline{x}(t) = \underline{\underline{\Phi}}(t,t_o)\,\underline{x}(t_o) + \int_{t_o}^{t} \underline{\underline{\Phi}}(t,\tau)\,\underline{b}u(\tau)\,d\tau \quad , \tag{15}$$

where $\underline{\underline{\Phi}}(t,\tau) = \exp\{\underline{\underline{A}}(t-\tau)\}$ is the state transition function. From Eq. (2) this last expression can be written as

$$\underline{x}(t) = \underline{\underline{\Phi}}(t,t_o)\,\underline{x}(t_o) + \sum_{k=N(t_o)+1}^{N(t)} \underline{\underline{\Phi}}(t,t_k)\,\underline{b}u_k \tag{16}$$

so that finally

$$\psi_g(v;t) = E\{\exp[iv\langle \underline{c}, \underline{\underline{\Phi}}(t,t_o)\,\underline{x}(t_o)\rangle]\}\; E\left\{\exp\left[iv \sum_{k=N(t_o)+1}^{N(t)} \langle \underline{c}, \underline{\underline{\Phi}}(t,t_k)\,\underline{b}\rangle u_k\right]\right\} \quad . \tag{17}$$

Let us give consideration to the evaluation of the second of these expectations. This quantity is easily seen to be the ch.f. of a random sum of independent although not necessarily identically distributed random variables. If the counting process $\{N(t),\ t \geq 0\}$ is assumed Poisson* with intensity λ, it can easily be shown[5] that

$$E\left\{\exp\left[iv \sum_{k=N(t_o)+1}^{N(t)} \langle \underline{c}, \underline{\underline{\Phi}}(t,t_k)\,\underline{b}\rangle u_k\right]\right\} = \exp\left\{\lambda \int_{t_o}^{t} [\varphi(v;\tau) - 1]\,d\tau\right\} \quad , \tag{18}$$

where

$$\varphi(v;\tau) = E\{\exp[iv\langle \underline{c}, \underline{\underline{\Phi}}(t,\tau)\,\underline{b}\rangle u]\} \tag{19}$$

---

*It is of some interest to extend these results to the case of an arbitrary renewal counting process.

is the ch.f. of the random term appearing in the summation of (14). Here the expectation is with respect to the only random quantity u so that

$$\varphi(v;\tau) = \psi_u(v\langle \underline{c}, \underline{\underline{\Phi}}(t,\tau)\,\underline{b}\rangle) \tag{20}$$

with $\psi_u(\cdot)$ the univariate ch.f. of the random amplitudes $\{u_k\}$ possessing common p.d.f. $f(\cdot)$. It will be convenient to let

$$h(t,\tau) = \langle \underline{c}, \underline{\underline{\Phi}}(t,\tau)\,\underline{b}\rangle \quad , \tag{21}$$

noting that $h(t,\tau) = h(t-\tau)$ due to the time invariance of $\underline{\underline{\Phi}}(t,\tau)$. Indeed, h(t) is easily seen to be the inverse Laplace Transform of the system transfer function H(s) in Eq. (5) and thus represents the impulse response of the linear time-invariant system.

Similarly, for the first expectation in (17) we obtain

$$E\{\exp[iv\langle \underline{c}, \underline{\underline{\Phi}}(t,t_o)\,\underline{x}(t_o)\rangle\}] = E\{\exp[i\langle v\underline{\underline{\Phi}}^{\dagger}(t,t_o)\,\underline{c}, \underline{x}(t_o)\rangle]\} \triangleq \psi_{\underline{x}(t_o)}(v\underline{\underline{\Phi}}^{\dagger}(t,t_o)\,\underline{c}) \tag{22}$$

with $\psi_{\underline{x}(t_o)}(\cdot)$ the multidimensional ch.f. of the initial state vector $\underline{x}(t_o)$, and where $\underline{\underline{\Phi}}^{\dagger}(t,t_o)$ denotes the conjugate transpose of the state-transition matrix. Thus, using the preceding results in (17), we obtain

$$\psi_y(v;t) = \psi_{\underline{x}(t_o)}(v\underline{\underline{\Phi}}^{\dagger}(t,t_o)\,\underline{c}) \exp\left\{\lambda \int_{t_o}^{t} [\psi_u(vh(t,\tau)) - 1]\,d\tau\right\} \tag{23}$$

for the ch.f. of the shot component. For a specified distribution of the initial state vector $\underline{x}(t_o)$ and the p.d.f. $f(\cdot)$ of the random amplitude, the ch.f.'s $\psi_{\underline{x}(t_o)}(\cdot)$ and $\psi_u(\cdot)$ are determined. The evaluation of $\psi_y(v;t)$ is then relatively straightforward, although possibly tedious, for specified system dynamics. The quantity $\psi_y(v;t)$ has been evaluated for some special cases in a previous memorandum.[9]

Also of some interest is the joint ch.f. of the shot component at times t_1, t_2 with $t_2 > t_1$ say. By a derivation similar to the above it is easily shown that this quantity is given by

$$\psi_y(\underline{v};t_1,t_2) = \psi_{\underline{x}(t_o)}([v_1\underline{\underline{\Phi}}^{\dagger}(t_1,t_o) + v_2\underline{\underline{\Phi}}^{\dagger}(t_2,t_o)]\,\underline{c}) \exp\left\{\lambda \int_{t_o}^{t_1} [\psi_u\{v_1 h(t,\tau) + v_2 h(t_2,\tau)\} - 1]\,d\tau\right\} \exp\left\{\lambda \int_{t_1}^{t_2} [\psi_u(v_2 h(t_2,\tau)) - 1]\,d\tau\right\} \quad , \tag{24}$$

where $\underline{v} = (v_1, v_2)$. This expression can again be evaluated for specified distributions on $\underline{x}(t_o)$ and u and assigned system dynamics.

It will be convenient in what follows to assume that we will be interested only in times that are sufficiently far removed from t_o so that initial transient disturbances have been dissipated. For all such times t we have approximately $\underline{\underline{\Phi}}^{\dagger}(t,t_o)\,\underline{c} \approx \underline{0}$, the null vector so that the following approximations are valid

$$\psi_y(v;t) \approx \exp\left\{\lambda \int_0^{\infty} [\psi_u(vh(\xi)) - 1]\,d\xi\right\} \tag{25}$$

and

$$\psi_y(\underline{v}; t_1, t_2) \approx \exp\left\{\lambda \int_0^\infty [\psi_u\{v_1 h(\xi) + v_2 h(\xi + \tau)\} - 1]\, d\xi\right\}$$

$$\times \exp\left\{\lambda \int_0^\tau [\psi_u(v_2 h(\xi)) - 1]\, d\xi\right\} \quad , \tag{26}$$

where $\tau = t_2 - t_1$. With $y(t) = \langle \underline{c}, \underline{x}(t) \rangle$ representing the shot component, it follows that

$$E\{y(t)\} = \lambda E\{u\} \int_0^\infty h(\xi)\, d\xi \quad . \tag{27}$$

Similarly, we have

$$\text{var}\{y(t)\} = \lambda E\{u^2\} \int_0^\infty h^2(\xi)\, d\xi \tag{28}$$

and for the autocorrelation function

$$R(\tau) = E\{y(t)\, y(t+\tau)\} = \lambda^2 E^2\{u\} \left[\int_0^\infty h(\xi)\, d\xi\right]^2 + \lambda E\{u^2\} \int_0^\infty h(\xi)\, h(\xi + \tau)\, d\xi \tag{29}$$

with corresponding spectral density function

$$S(\omega) = 2\pi\lambda^2 E^2\{u\}\, H^2(0)\, \delta(\omega) + \lambda E\{u^2\}\, |H(j\omega)|^2 \quad , \tag{30}$$

where $H(j\omega)$ is the Fourier Transform of $h(t)$, i.e., the system transfer function $H(s)$ evaluated at $s = j\omega$ provided that the imaginary axis is within the region of absolute convergence of $H(s)$. Table II summarizes the properties of several linear systems which will be of interest to us in

TABLE II

MEAN AND VARIANCE OF SHOT COMPONENT
FOR SOME USEFUL SYSTEM TRANSFER FUNCTIONS

$H(s)$	$h(t)$	$E\{y(t)\}$	$\text{Var}\{y(t)\}$
$\frac{c}{s+a}$	$ce^{-at}u_{-1}(t)$	$\frac{\lambda c E\{u\}}{a}$	$\frac{\lambda c^2 E\{u^2\}}{2a}$
$\frac{c}{(s+a)^2+\omega^2}$	$\frac{ce^{-at}}{\omega}\sin\omega t\, u_{-1}(t)$	$\frac{\lambda c E\{u\}}{a^2+\omega^2}$	$\frac{\lambda c^2 E\{u^2\}}{4a(a^2+\omega^2)}$
$\frac{c(s+a)}{(s+a)^2+\omega^2}$	$ce^{-at}\cos\omega t\, u_{-1}(t)$	$\frac{\lambda a c E\{u\}}{a^2+\omega^2}$	$\frac{\lambda c^2 \omega^2 E\{u^2\}}{4a(a^2+\omega^2)}$

what follows. We will for the most part be interested only in the case where $E\{u\} = 0$. From Table II, then, it is a simple matter to choose the value c for specified system dynamics to achieve a given value of γ defined by

$$\gamma^2 = \frac{\text{var}\{y(t)\}}{\sigma_o^2} \tag{31}$$

i.e., γ represents the ratio of the rms value of the shot noise component to that of the additive

background Gaussian noise and will prove to be an important parameter of the proposed model.

In summary, then, the parameters of the proposed model which must be specified are:

(a) The p.d.f. $f(\cdot)$ of the pulse amplitudes,

(b) The intensity λ of the Poisson point process,

(c) The linear system dynamics,

(d) The ratio γ of the rms values of the shot and Gaussian components.

Observe that the choice of background noise level σ_o^2 is somewhat arbitrary and merely amounts to a trivial rescaling of the process n(t). As a result, we will assume $\sigma_o^2 = 1$ in what follows. In the following sections we will discuss the choice of the above parameters to match observed ELF noise.

IV. DIGITAL REALIZATION OF MODEL FOR ELF H-FIELD NOISE

We will be particularly concerned with fitting the model described in the preceding section to observed H-field data and obtaining a suitable digital realization of this model. The situation is complicated somewhat by the fact that the available noise data have been recorded with a loop antenna, thus measuring the time derivative of the ambient H-field. To compensate for this, the raw data are processed by a filter with an attenuation characteristic exhibiting a 6 dB/octave roll-off out to 350 Hz. This approximate integration reconstructs a facsimile of the actual H-field data. We will approximate this filter by a moving average operation performed on the

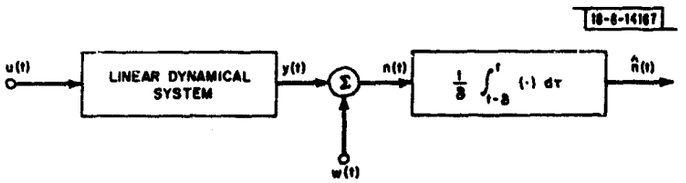

Fig. 11. Model of observed H-field data.

n(t) process as illustrated in Fig. 11. The resulting process $\hat{n}(t)$ is then related to the n(t) process of the previous section by

$$\hat{n}(t) = \frac{1}{\delta}\int_{t-\delta}^{t} n(\tau)\,d\tau \quad . \tag{32}$$

This operation can be considered as the convolution of the input n(t) with the impulse response

$$h_I(t) = \frac{1}{\delta}\left[u_{-1}(t) - u_{-1}(t-\delta)\right] \quad , \tag{33}$$

where $u_{-1}(t)$ is the unit step function. The corresponding squared-magnitude response is given by

$$|H_I(\omega)|^2 = \left[\frac{\sin \omega\delta/2}{\omega\delta/2}\right]^2 \quad , \tag{34}$$

which is down 3 dB at $\omega = \omega_o \triangleq 2.78/\delta$. It is reasonable then to adjust the average interval δ to result in a "bandwidth" $\omega_o = 2\pi \times 350$ rad/sec.* We will assume then that

* Later studies have indicated that δ should be made somewhat larger than this value to result in spectral characteristics which more closely resemble observed ELF H-field noise.

$$\delta = \frac{1}{2\pi}\left(\frac{2,78}{350}\right) \tag{35}$$

in what follows.

The digital simulation of the input/output behavior of the linear dynamical system is determined from the following considerations. Observe that the solution to the state equation (1a) is given for any $t > \tau$ by

$$\underline{x}(t) = \underline{\Phi}(t, \tau)\,\underline{x}(\tau) + \int_{\tau}^{t} \underline{\Phi}(t, \xi)\,\underline{b}u(\xi)\,d\xi \quad , \tag{36}$$

where $\underline{\Phi}(t, \tau) = \exp\{\underline{A}(t - \tau)\}$ as has been described previously. Thus, if we are interested only in the discrete times $t = k\Delta$, $k = 0, 1, 2, \ldots$, where Δ is the sampling interval, we have upon letting $\underline{x}_k = \underline{x}(k\Delta)$ the discrete recurrence relation

$$\underline{x}_{k+1} = \underline{F}\,\underline{x}_k + \tilde{\underline{b}}_k \tilde{u}_{k+1} \quad ; \quad \underline{x}_o = \underline{0} \quad , \tag{37a}$$

$$y_k = \langle \underline{c}, \underline{x}_k \rangle \quad , \tag{37b}$$

where $\underline{F} = \exp\{\underline{A}\,\Delta\}$, and

$$\tilde{u}_{k+1} = \begin{cases} 0 & \text{if no impulse occurred in the interval } (k\Delta,\ (k+1)\,\Delta] \\ u_i & \text{if the } i^{th} \text{ impulse occurred at time } t_i,\ k\Delta < t_i \leq (k+1)\,\Delta \end{cases} \quad . \tag{38}$$

Finally, $\tilde{\underline{b}}_k$ is defined only for nonzero $\tilde{u}_k$ values as $\tilde{\underline{b}}_k = \exp\{\underline{A}[(k+1)\,\Delta - t_i]\}\,\underline{b}$. Thus, taking z-transforms in (37), we have for the discrete transfer function

$$H(z) = \frac{Y(z)}{\tilde{U}(z)} = \langle \underline{c}, [\underline{I} - z^{-1}\underline{F}]^{-1}\,\tilde{\underline{b}} \rangle \quad , \tag{39}$$

where $\tilde{U}(z)$ and $Y(z)$ are the z-transforms of the input and output sequences $\{\tilde{u}_k\}$ and $\{y_k\}$, respectively. We shall assume that the sampling interval Δ is small relative to any time constants associated with the linear system so that* $\tilde{\underline{b}} \approx \underline{b}$. Again making use of the spectral representation[8] we have

$$[\underline{I} - z^{-1}\underline{F}]^{-1} = \sum_{k=1}^{n} \frac{\underline{Z}_k}{1 - z^{-1} e^{s_k \Delta}} \quad , \tag{40}$$

where the s_k, $k = 1, 2, \ldots n$ are again poles of $H(s)$, and the $\underline{Z}_k$ are defined as in Eq. (6) and the sequel. It follows that the discrete transfer function $H(z)$ can be expressed as

$$H(z) = \sum_{k=1}^{n} \frac{A_k}{1 - z^{-1} e^{s_k \Delta}} \tag{41}$$

with A_k $k = 1, 2, \ldots n$, again the residues of $H(s)$ at the distinct poles s_k, $k = 1, 2, \ldots n$. This is the essence of the impulse invariance technique of digital filtering[10] and results in a parallel realization of the discrete system described by (37). In the present study, we have concentrated upon the three linear systems described in Table II for which the parallel digital realizations

*At any rate, in the digital simulation the impulses occurring at $k\Delta < t_i \leq (k+1)\,\Delta$ will always be placed at the right-hand boundary of such intervals so that this approximation is exact.

corresponding to (41) are readily obtained. A FORTRAN program for a complete digital simulation of the proposed model has been written and used extensively in this study.

V. CHOICE OF PARAMETER VALUES

The first quantity to be specified for the proposed model is, of course, the p.d.f. $f(\cdot)$ of the individual pulse amplitudes. In principle, this information could be obtained from the results of Section III by computing the APD from the derived expressions for the ch.f. for a specific choice of $f(\cdot)$ and comparing the results with measured APD's. The difficulty in actually computing the APD except in special cases, however, precludes this approach. As an alternative, let us note that the APD at high levels should essentially be determined by the large noise peaks and hence should resemble $f(\cdot)$. Let us then choose a p.d.f. whose amplitude distribution at large levels is similar to that observed in measured APD's. We have considered two such zero-mean distributions which appear to satisfy this requirement: the double-sided power-Rayleigh distribution defined by

$$f(u) = \frac{\alpha |u|^{\alpha-1}}{2R_o^{\alpha}} \exp\left\{-\left|\frac{u}{R_o}\right|^{\alpha}\right\} \quad ; \quad 0 < \alpha \leq 2 \tag{42}$$

and the double-sided log-normal distribution defined by*

$$f(u) = \frac{1}{2\sqrt{2\pi}\,\sigma\,|u|} \exp\left\{-\frac{(\ell n|u| - \mu)^2}{2\sigma^2}\right\} \quad , \tag{43}$$

where μ and σ^2 are the mean and variance, respectively, of a Gaussian variate g for which $u = e^g$. In particular, we will assume that $\mu = 0$ in what follows. The power-Rayleigh distribution has a variance $R_o^2\,\Gamma(1 + 2/\alpha)$, where $\Gamma(\cdot)$ is the Gamma function while the log-normal distribution possesses a variance $\exp\{2\sigma^2\}$. Thus, the power-Rayleigh distribution is completely defined by the scale parameter R_o and the exponent α. A plot of the resulting APD for the power-Rayleigh distribution is illustrated in Fig. 12 for several values of α. By comparison with the high-level region of the measured APD plots given in Figs. 4 through 6, values of α in the range $0.25 \leq \alpha \leq 0.50$ have been found appropriate. Similarly, we have found it useful to characterize the log-normal distribution by the scale parameter σ and the related quantity

$$V_d = 10 \log_{10} \frac{E\{u^2\}}{E^2\{|u|\}} = 4.34\,\sigma^2 \quad . \tag{44}$$

Plots of the resulting APD for several values of V_d are illustrated in Fig. 13. Here it appears that values of V_d in the range $10 \leq V_d \leq 15$ prove sufficient.

Now let us consider appropriate choices for the intensity λ of the point process. This information can be obtained directly from the data of Table I. For definiteness we will take λ as the average number of high-level pulses per second from Table I with $S_c = 5$ msec as this choice appears to correlate most favorably with visual observations. Additional information on system

*Each of these distributions can be obtained by forming the random variable $u = pr$, where r has a conventional one-sided distribution of either type and p is a random variable taking values ± 1 with equal probability.

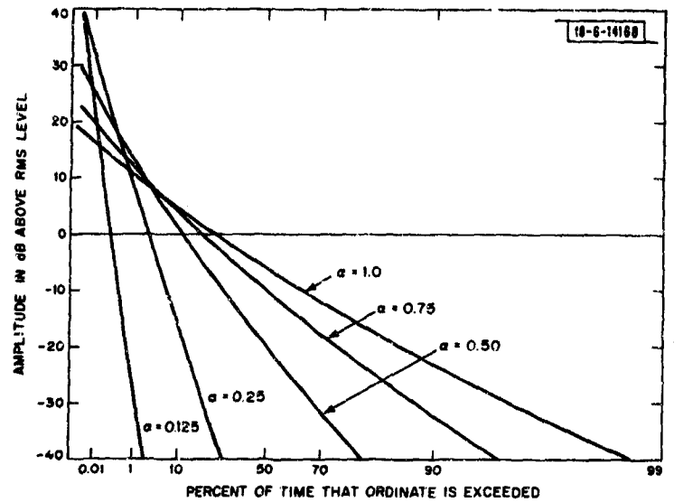

Fig. 12. APD of double-sided power-Rayleigh distribution.

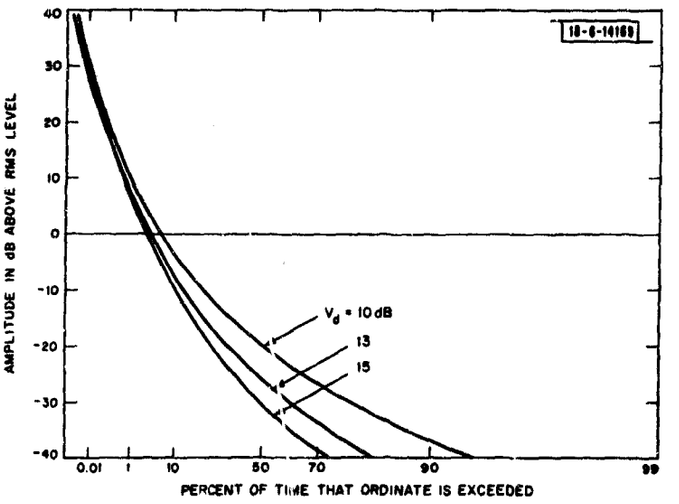

Fig. 13. APD of double-sided log-normal distribution.

dynamics can be gleaned from Table I. In particular, each of the linear system transfer functions in Table II possesses an impulse response with a well-defined duration (or time-constant) $T_c = 1/a$ seconds. It then proves convenient in each case to adjust the parameter a to provide an average pulse duration as given by the measured data in Table I. Again for definiteness we take the average pulse duration with $S_c = 5$ msec as this choice correlates most favorably with visual observations. For system transfer functions with complex poles, it has been determined that $\omega \approx 2000$ rad/sec should prove sufficient in each case considered. Thus, all that remains is to develop an appropriate rationale for choice of the quantity γ given by (31). This in turn follows easily from consideration of the effect of the parameter γ on a typical APD plot. As we have previously observed, the APD is controlled mainly by the background Gaussian noise in the small signal regime. Thus, by observing the amount by which the straight-line segments of the APD plots in the small-signal regime are depressed below the APD corresponding to Gaussian noise alone (Fig. 7), we should be able to obtain a rough estimate of γ. In particular, observe

$$\frac{r}{\sigma} = \frac{r/\sigma_o}{\sqrt{1 + \gamma^2}} \quad , \tag{45}$$

where we have made use of the fact $\sigma^2 = \sigma_o^2(1 + \gamma^2)$. Thus, the amount by which the APD should be depressed below that for Gaussian noise alone is given by

$$\Delta_{dB} = 10 \log_{10}(1 + \gamma^2) \quad . \tag{46}$$

It should be noted that this approximation can be expected to hold only for γ sufficiently greater than unity. As an example, comparing Fig. 4 with Fig. 7, it is observed that the low-level Gaussian segment of the former is depressed by $\Delta_{dB} \approx 13$ so that $\gamma = 4.4$. In cases where the approximation fails, resort has been made to visual observation of the resulting APD plots for choice of γ.

Table III indicates the appropriate choice of parameter values for each of the models considered and has been generated by the above procedure. As an example of the type of results to be obtained, consider the high-level Saipan data. Figures 14 through 19 illustrate typical noise waveforms obtained from the proposed model with parameter values taken from Table III. These waveforms should be compared with that in Fig. 1. Observe that the most favorable visual correspondence is obtained with a linear system possessing a pair of complex conjugate poles. We have, nevertheless, decided not to neglect entirely the single-pole model as it is felt that this simplified model may have some utility in later studies – in particular, in the digital computer simulation of optimum detector structures. It has been determined that the resulting APD plots for the artificially generated ELF noise do not exhibit noticeable differences for the different linear system used to generate the shot process, provided that the other parameters remain fixed. Figures 20(a) and 20(b) illustrate the correspondence between the APD's of artificially generated and recorded high-level Saipan data when the parameters of the proposed model are chosen from Table III. As can be observed, the correspondence is extremely good. Similar correspondences have been obtained with the Malta and Norway data.

As a final comment, it should be noted that some estimate of the processing gains to be realized with typical nonlinear receiver structures operating upon noise as described by this

TABLE III

PARAMETER VALUES FOR ELF H-FIELD NOISE MODEL

Noise Data	λ(pulses/sec)	a(sec^{-1})	ω(rad/sec)	Power-Rayleigh Distributed Pulse Amplitudes			Log-Normal Distributed Pulse Amplitudes		
				α	γ	Δ_{dB}	V_d	γ	Δ_{dB}
Saipan									
High-Level	12.8	250	2000	0.25	4.4	13.0	15	4.4	13.0
Moderate-Level	10.2	200	2000	0.25	3.0	10.0	15	2.0	7.0
Low-Level	8.0	166	2000	0.50	1.2	3.8	13	1.0	3.0
Malta									
High-Level*									
Moderate-Level	11.3	250	2000	0.25	2.6	8.9	15	2.0	7.0
Low-Level*									
Norway	9.3	333	2000	0.50	1.2	3.8	13	1.0	3.0

* No data available.

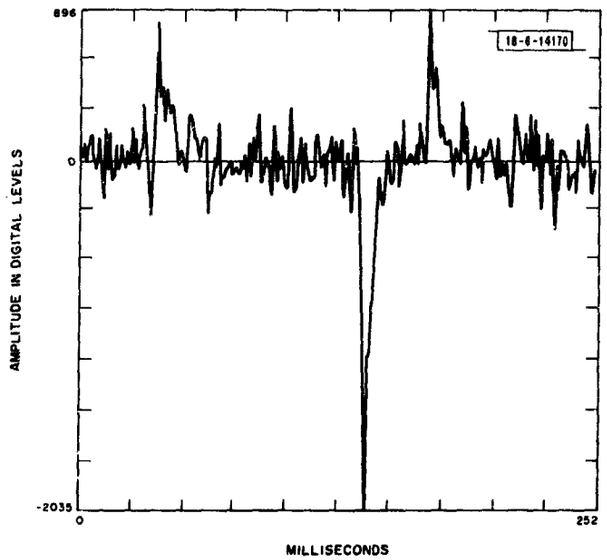

Fig. 14. Simulated noise waveform: single-pole model with power-Rayleigh distributed pulse amplitudes.

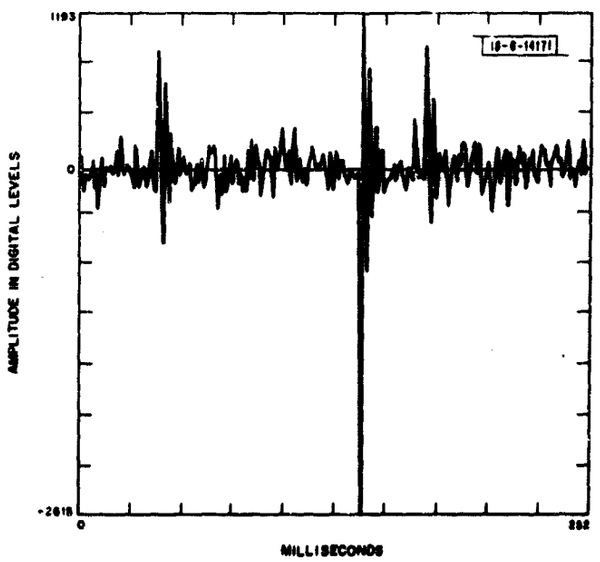

Fig. 15. Simulated noise waveform: two-pole model with power-Rayleigh distributed pulse amplitudes.

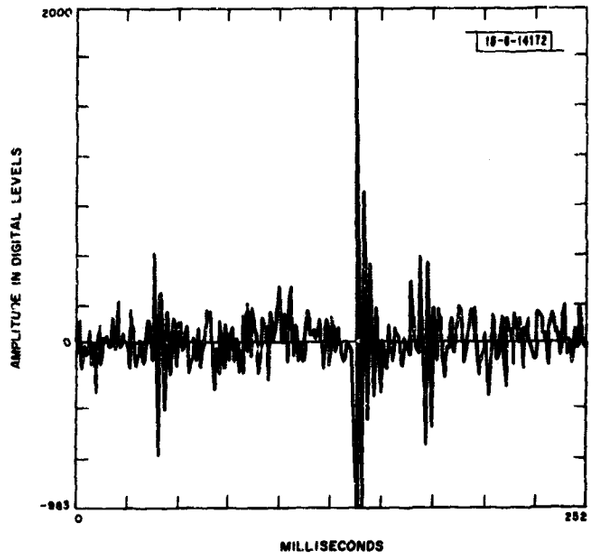

Fig. 16. Simulated noise waveform: two-pole, single zero model with power-Rayleigh distributed pulse amplitudes.

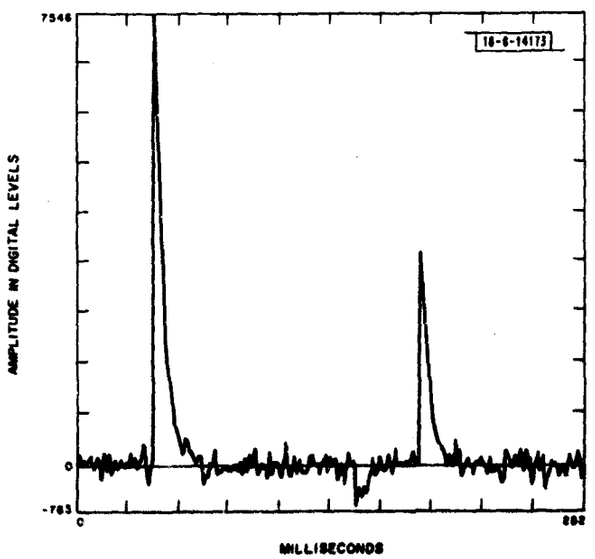

Fig. 17. Simulated noise waveform: single-pole model with log-normal distributed pulse amplitudes.

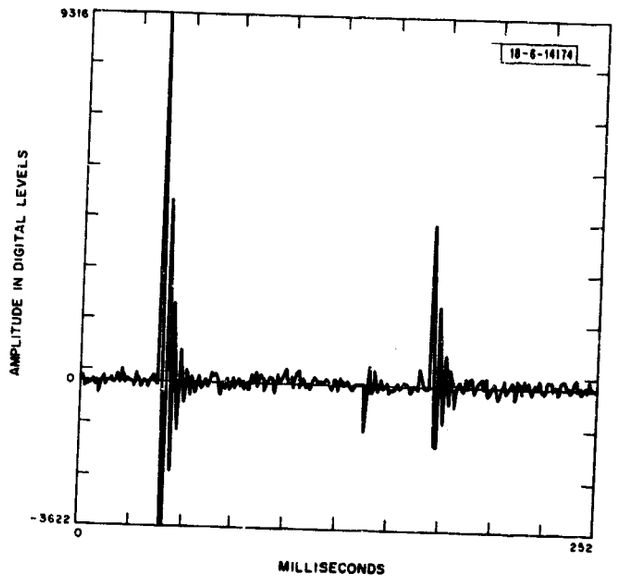

Fig. 18. Simulated noise waveform: two-pole model with log-normal distributed pulse amplitudes.

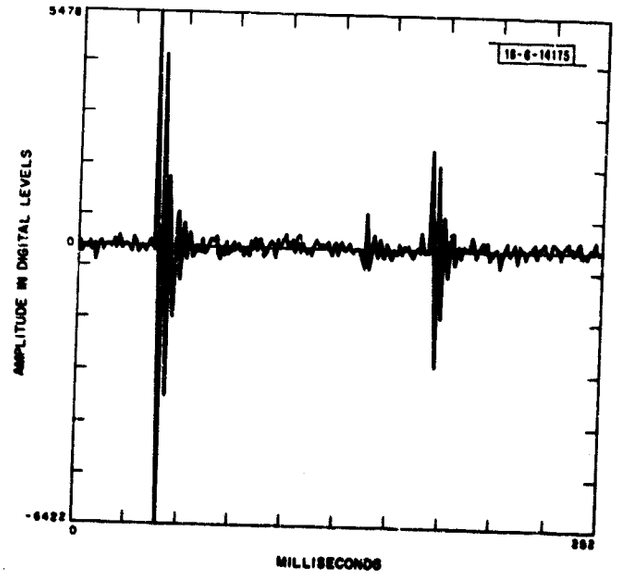

Fig. 19. Simulated noise waveform: two-pole, single zero model with log-normal distributed pulse amplitudes.

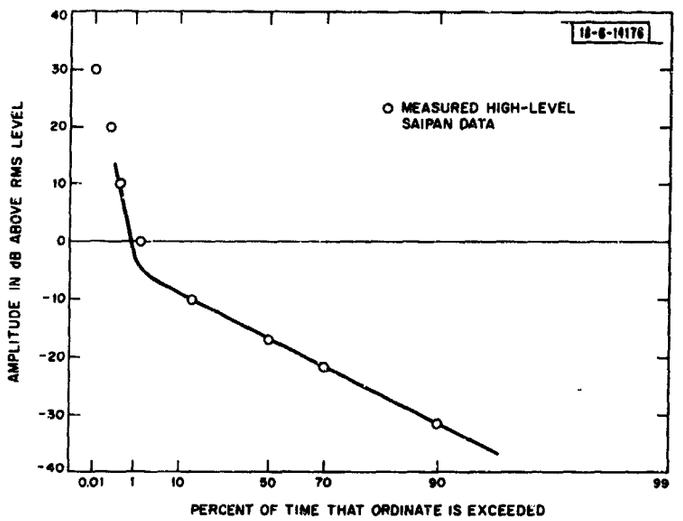

(a) Power-Rayleigh distributed pulse amplitudes.

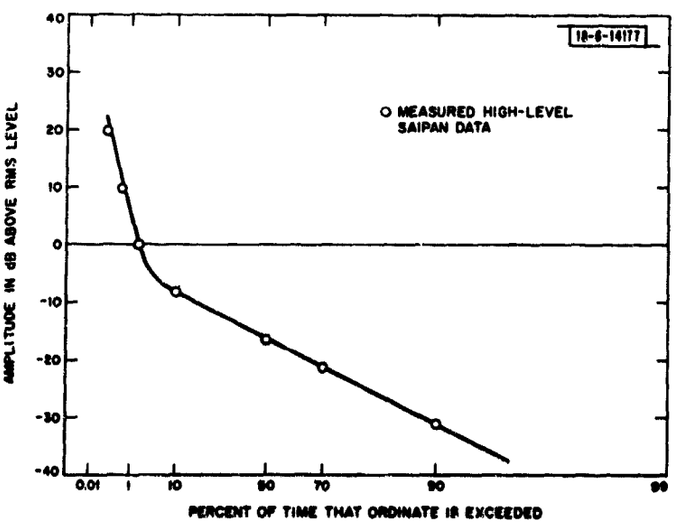

(b) Log-normal distributed pulse amplitudes.

Fig. 20. Correspondence between APD of ELF noise model and measured data.

model can be obtained from the data of Table III. In particular, consider a detector of the hole-punching variety with threshold set just above the background Gaussian noise level.* The fraction of signal energy lost in any 1-second interval is approximately λT_c which, from the data of Table III, is negligible in each case. The reduction of noise power, on the other hand, is approximately given by Δ_{dB} as defined in (46). Thus, the processing gain is approximately Δ_{dB} which, in each of the cases considered, has been included in Table III. This estimate comes surprisingly close to the processing gain measured with corresponding recorded noise data.

VI. SUMMARY AND CONCLUSIONS

A model for ELF noise has been proposed and studied in detail. A procedure has been given for fitting the free parameters of this model to observed noise data. It is felt that the model satisfies all the diserata listed in Section I. Further studies will be concerned with the determination of optimum/suboptimum detector structures for reception in noise as described by this model and the evaluation of the resulting performance.

There are several directions in which the proposed model could be generalized to more closely represent observed ELF noise. For instance, the Poisson point process could be replaced by one which would result in some correlation between noise burst intervals as has been observed in recorded data. Another possibility is to consider linear systems with multiple-order poles for generating the low-density shot processes. This would result in pulse waveforms possessing observable precursors which again have been observed in recorded data. Such refinements were not undertaken in the present study.

REFERENCES

1. J. E. Evans, "Preliminary Analysis of ELF Noise," Technical Note 1969-18, Lincoln Laboratory, M.I.T. (26 March 1969), DDC AD-691814.
2. A. Papoulis, Probability, Random Variables and Stochastic Processes (McGraw-Hill, New York, 1965), Chap. 16.
3. E.N. Gilbert and H.O. Pollak, "Amplitude Distribution of Shot Noise," Bell System Tech. J. 39, 333-350 (1960).
4. D.L. Snyder, "Optimal Detection of Known Signals in a Non-Gaussian Noise Resembling VLF Atmospheric Noise," 1968 Wescon Convention Record, Part 4.
5. E. Parzen, Stochastic Processes (Holden-Day, San Francisco, 1962), Chap. 4.
6. L. Zadeh and C. Desoer, Linear System Theory (McGraw-Hill, New York, 1963).
7. D.L. Snyder, The State-Variable Approach to Continuous Estimation, Research Monograph No. 51 (M.I.T. Press, Cambridge, 1969).
8. P. Lancaster, Theory of Matrices (Academic, New York, 1969), Chap. 5.
9. J.W. Modestino, "Comments on Models for ELF Atmospheric Noise," unpublished Lincoln Laboratory memorandum, April 1971.
10. B. Gold and C.M. Rader, Digital Processing of Signals (McGraw-Hill, New York, 1969), Chap. 3.

* In particular, at the level T defined in Section II.